# Supplemental Information

A. M. Jayich,* X. Long, and W. C. Campbell
*UCLA Department of Physics and Astronomy, Los Angeles, California 90095, USA and*
*California Institute for Quantum Emulation, Santa Barbara, California 93106, USA*
(Dated: July 5, 2016)

## FREQUENCY LOCK FOR THE OPTICAL FREQUENCY COMB

To tune the ML laser near the resonance condition for the $5S \rightarrow 5D$ two-photon transition in rubidium (Fig. 2 in the main text), we sample a fraction of the laser power and send it to a hot Rb vapor cell in a counter-propagating geometry [1]. Each excitation to the $5^2D_{5/2}$ state produces a spontaneously emitted 420 nm photon as part of a cascade decay 6.5% of the time (Fig. 2**c** in the main text), which is collected from the pulse collision volume and monitored with a photon-counting detector. Fig. 2**a** in the main text shows the resulting Doppler-free spectrum of the 32 allowed two-photon transitions for both $^{85}$Rb and $^{87}$Rb from the $5S$ to $5D$ manifolds. Since the bandwidth of the comb ($< 500$ GHz) is smaller than the detuning from 1-photon resonance with the $5P$ states ($\Delta/2\pi > 1$ THz), the spectrum repeats itself with a (two-photon sum frequency) period of $f_\mathrm{r}$. We laser cool and trap $^{85}$Rb using the $5^2S_{1/2}, F_\mathrm{g} = 3$ to $5^2D_{5/2}, F_\mathrm{e} = 5$ "stretch" transition.

To maintain sufficient laser stability for Doppler cooling and trapping, we stabilize the ML laser by locking it to an external cavity. The free spectral range of the external cavity is pressure tuned to be an integer multiple ($q = 25$) of the ML laser repetition rate to guarantee that multiple teeth from across the laser spectrum contribute to the Pound-Drever-Hall error signal used for the lock. A piezo-mounted mirror on the external cavity is then used to stabilize it to the $5^2S_{1/2}, F_\mathrm{g} = 3$ to $5^2D_{5/2}, F_\mathrm{e} = 5$ line using FM spectroscopy of the vapor cell. We note that this optical frequency comb is not self referenced and that we feed back to an unknown combination of $f_\mathrm{r}$ and $f_0$ to maintain the two-photon resonance condition, which is the only frequency parameter that needs to be actively stabilized. The pulse chirp is periodically minimized by adjusting a Gires-Tournois interferometer in the laser cavity to maximize the blue light emitted from atoms in the initial CW MOT. The frequency of the ML laser light used for cooling and trapping is tuned from the vapor cell lock point using an acousto-optic modulator downstream.

## EFFECTIVE TWO-PHOTON RABI FREQUENCY

We model the electric field of a frequency comb propagating along $+z$ in the plane wave approximation as

$$\mathbf{E}(z,t) = \frac{\mathcal{E}_\mathrm{o}}{2}\mathrm{Env}(t)\sum_q h(t-qT_\mathrm{r})\left(\hat{\boldsymbol{\epsilon}}\, e^{-i(2\pi f_\mathrm{c}(t-qT_\mathrm{r})+q2\pi f_0 T_\mathrm{r}-kz)} + \hat{\boldsymbol{\epsilon}}^* e^{i(2\pi f_\mathrm{c}(t-qT_\mathrm{r})+q2\pi f_0 T_\mathrm{r}-kz)}\right) \tag{S1}$$

where $\mathrm{Env}(t)$ is the slowly-varying envelope of the pulse train (we will take this to be equal to 1), $\mathcal{E}_\mathrm{o}h(0)$ is the peak instantaneous electric field amplitude, $h(t)$ is the envelope of a single pulse (peaked at $t = 0$), $\hat{\boldsymbol{\epsilon}}$ is the unit vector describing the laser polarization, $f_\mathrm{c}$ is the carrier frequency of the laser and $f_0$ is the carrier-envelope offset frequency. If the pulse envelope $h(t)$ is real and symmetric about $t = 0$ with Fourier transform $\tilde{\mathrm{H}}(\omega)$, we can rewrite Eq. (S1) as

$$\mathbf{E}(z,t) = \sum_p \frac{\mathcal{E}_p}{2}\left(\hat{\boldsymbol{\epsilon}} e^{-i(2\pi f_p t-kz)} + \hat{\boldsymbol{\epsilon}}^* e^{i(2\pi f_p t-kz)}\right) \tag{S2}$$

where $f_p \equiv pf_\mathrm{r} + f_0$ is the cyclic frequency of the $p^\mathrm{th}$ optical frequency comb tooth and

$$\mathcal{E}_p = \mathcal{E}_\mathrm{o}\frac{\tilde{\mathrm{H}}(2\pi(f_p - f_\mathrm{c}))}{T_\mathrm{r}} \tag{S3}$$

is the time-averaged electric field amplitude of the $p^\mathrm{th}$ optical frequency comb tooth. The single-photon resonant Rabi frequency for just the $p^\mathrm{th}$ tooth to drive the $\mathrm{g} \rightarrow \mathrm{i}$ transition is given by

$$g_p^{(\mathrm{gi})} = \frac{e\mathcal{E}_p}{\hbar}\langle \mathrm{i}|\hat{\boldsymbol{\epsilon}}\cdot\mathbf{r}|\mathrm{g}\rangle \tag{S4}$$

* jayich@gmail.com

(where $\mathbf{r}$ is the position operator for the electron) and likewise for $\mathrm{i}\rightarrow\mathrm{e}$, which appear in Eq. (1) in the main text as $g^{(1)}$ and $g^{(2)}$, respectively.

The $5^2S_{1/2}\rightarrow 5^2D_{5/2}$ two-photon transition near 778 nm in rubidium primarily gets its strength through single-photon couplings to the nearby $5^2P_{3/2}$ state, which approximation was made implicitly in Eq. (1) in the main text. For the more general case, the $\mathrm{g}\rightarrow\mathrm{e}$ two-photon Rabi frequency includes a sum over all of the possible intermediate states $\{|\mathrm{i}\rangle\}$. Matrix elements for calculating AC Stark shifts and photoionization are similar, but include single photon detunings $\Delta$ for both emission first and absorption first. In the case of hydrogen, it is even important to include continuum states in the sum over i, which contribute substantially [2]. The two-photon resonant Rabi frequency associated with the $n^{\mathrm{th}}$ tooth of the "two-photon" comb can be written

$$\Omega_n = \sum_p \frac{e^2\mathcal{E}_p\mathcal{E}_{n-p}}{\hbar^2}\langle \mathrm{e}|(\hat{\boldsymbol{\epsilon}}\cdot\mathbf{r})\left(\sum_{\mathrm{i}}\frac{|\mathrm{i}\rangle\langle\mathrm{i}|}{2\Delta_p^{(\mathrm{i})}}\right)(\hat{\boldsymbol{\epsilon}}\cdot\mathbf{r})|\mathrm{g}\rangle. \tag{S5}$$

For a comb whose spectrum is centered approximately halfway between $|\mathrm{e}\rangle$ and $|\mathrm{g}\rangle$, the time-averaged laser intensity $I$ is related to this via $\sum_p \mathcal{E}_p\mathcal{E}_{n-p} \approx 2I/\epsilon_{\mathrm{o}}c$.

In the limit that all of the single-photon detunings $\Delta_p^{(\mathrm{i})}$ are much larger than the fine and hyperfine splittings (which is often valid, but is not applicable for the 778 nm line in rubidium), since the term in parentheses includes a sum over all possible projection quantum numbers, it is rotationally invariant and the angular momentum prefactors for calculating $\Omega_n$ arise entirely from the tensor $(\hat{\boldsymbol{\epsilon}}\cdot\mathbf{r})(\hat{\boldsymbol{\epsilon}}\cdot\mathbf{r})$. This limit holds well for hydrogen, and the tensor products can be used to calculate direct two-photon matrix elements between single quantum states by using the Wigner-Eckhart theorem and a single reduced matrix element [2]. Each irreducible spherical tensor component contained in $(\hat{\boldsymbol{\epsilon}}\cdot\mathbf{r})(\hat{\boldsymbol{\epsilon}}\cdot\mathbf{r})$ can be factored into the product of a polarization-independent term that contracts $\mathbf{r}$ with itself and an atom-independent term that depends only on the polarization, $\mathrm{T}^{(k)}[\hat{\boldsymbol{\epsilon}},\hat{\boldsymbol{\epsilon}}]$, which is known as the polarization tensor [3]. The rank 0 tensor product $\mathrm{T}^{(0)}[\mathbf{r},\mathbf{r}]$ is responsible for ${}^2S_{1/2}\rightarrow{}^2S_{1/2}$ transitions, while the rank 2 tensor $\mathrm{T}^{(2)}[\mathbf{r},\mathbf{r}]$ gives rise to the $S\rightarrow D$ transition amplitude in analogy to an electric quadrupole interacting with an electric field gradient. Reduced matrix elements for two-photon transitions and ionization rates in hydrogen have been calculated by Haas *et al.* [2] for linearly polarized light, and therefore include the value of the polarization tensor for linear $(\hat{\boldsymbol{\epsilon}}=\hat{\mathbf{z}})$ polarization $\mathrm{T}^{(k)}[\hat{\mathbf{z}},\hat{\mathbf{z}}]$.

In order to use these reduced matrix elements for the case of $\sigma^+$ or $\sigma^-$ light, they need to be scaled to reflect the change of the polarization tensor. This scaling factor is the term responsible for the increased strength of the $\sigma^+$ or $\sigma^-$ transitions as compared to $\pi$ polarizations. For $1S\rightarrow 3D$, there is a convenient comb repetition rate ($f_{\mathrm{r}} = 83.5$ MHz, see Fig. S1) such that all of the possible fine and hyperfine transitions of $1S\rightarrow 3D$ can be driven simultaneously. For a single $\sigma^+$ (or $\sigma^-$) polarized comb on two-photon resonance for $1S\rightarrow 3D$ stretch transitions with unresolved fine and hyperfine structure, we use the reduced matrix element $\beta_{ge}^{(2)}$ of Ref. [2] times the ratio of the circular to linear rank 2 polarization tensor components ($=\sqrt{6}/2$) to calculate the two-photon resonant Rabi frequency,

$$\Omega/2\pi = -6.8\, I\times 10^{-5}\ \mathrm{Hz}(\mathrm{W/m^2})^{-1}. \tag{S6}$$

Likewise, the ionization rate is given by the ionization rate for the $3D$ state times the fraction of atoms that are in the $3D$ state ($\approx\Omega^2/\gamma^2$):

$$\gamma_{\mathrm{ionization}}/2\pi = I\frac{\Omega^2}{\gamma^2}\,1.9\times 10^{-6}\ \mathrm{Hz}(\mathrm{W/m^2})^{-1} \tag{S7}$$

where $\gamma/2\pi = 10.3$ MHz is the $3D$ state decay rate and we have used the reduced matrix elements provided by Ref. [2] rescaled to reflect the value of $\mathrm{T}_0^{(2)}[\hat{\boldsymbol{\epsilon}},\hat{\boldsymbol{\epsilon}}^*]/\mathrm{T}_0^{(2)}[\hat{\mathbf{z}},\hat{\mathbf{z}}] = -1/2$.

## SCATTERING RATE FROM A FREQUENCY COMB

To estimate the scattering rate from a frequency comb of coupling strength $\Omega$ between a ground and excited state (whether it is due to a single or multi-photon process), we define the resonant saturation parameter for the $n^{\mathrm{th}}$ comb tooth to be $s_n \equiv 2\Omega_n^2/\gamma^2$, where $\gamma$ is the decay rate of the excited state, which we will model as decaying only to the ground state. We focus on the limit where $s_n \ll 1$ and $\Omega_n T_{\mathrm{r}} \ll \pi$ due to the low Rabi frequency expected for two-photon transitions under realistic experimental conditions. For optical forces, we are typically most interested in the time-averaged scattering rate, which permits us to simplify the model by summing up the scattering rates due

to each comb tooth instead of the excitation amplitudes. Specifically, the steady-state time-averaged scattering rate from the $n^{\text{th}}$ comb tooth by a stationary atom will be given by

$$\gamma_n \approx \gamma \frac{s_n}{2} \frac{1}{1 + (2\delta_n/\gamma)^2} \tag{S8}$$

where $\delta_n \equiv 2\pi(f_n - f_{\text{ge}})$ is the detuning of the $n^{\text{th}}$ comb tooth from resonance. If the center frequency of the comb of coupling strength is near $f_{\text{ge}}$ and the pulse duration is short compared to the excited state lifetime, $s_n$ will change very little over the range of $n$ that is within a few $\gamma$ of resonance and we can approximate $s_n = s_N$ where $N$ is the index of the comb tooth closest to resonance. In this case, we can use the identity

$$\sum_{n=-\infty}^{\infty} \frac{1}{1 + a^2(n-b)^2} = \frac{\pi}{a} \frac{\sinh(2\pi/a)}{\cosh(2\pi/a) - \cos(2\pi b)} \tag{S9}$$

to write

$$\gamma_{\text{comb}} = \sum_n \gamma_n = \gamma \frac{s_N}{2} \frac{(\gamma\, T_{\text{r}}/4)\sinh(\gamma\, T_{\text{r}}/2)}{\cosh(\gamma\, T_{\text{r}}/2) - \cos(\delta_N T_{\text{r}})}. \tag{S10}$$

In the limit where both $\delta_N/2\pi$ and $\gamma/2\pi$ are small compared to the repetition rate $f_{\text{r}}$, Eq. (S10) reduces to Eq. (S8) with $\gamma_{\text{comb}} \approx \gamma_N$. For the laser cooling and trapping we report with rubidium, the combined effect of all of the off-resonant comb teeth to the scattering rate when $\delta_N = -\gamma/2$ is approximately $10^{-4}\gamma_N$, and we can neglect their presence for slow-moving atoms. For hydrogen laser cooling on $1S{\rightarrow}3D$ at $f_{\text{r}} = 83.5$ MHz, this fraction is less than 0.04, and the single-tooth approximation is likely to be fair.

## ESTIMATES FOR APPLICATION TO HYDROGEN

For H and $\bar{\text{H}}$, two-photon Doppler cooling has previously been proposed on the $1S{\rightarrow}2S$ transition (through forced quenching of the $2S$ state) with a CW laser [4] or optical frequency comb [5] centered at 243 nm. Photoionization from the $2S$ state sets a limit on the intensity and effective (quenched) linewidth for this scheme, which ultimately limits the scattering rate. The photoionization cross section of the $3D$ state is approximately two orders of magnitude smaller than the $2S$ state for photons at half the state energy [2]. We therefore estimate parameters here for two-photon cooling on $1S{\rightarrow}3D$ at 205.0 nm, which is within the phase matching window for production by frequency doubling in BBO. We propose that the added difficulty of producing light at this deeper UV wavelength is justified by the lower photoionization rate and is further mitigated by the fact that for this transition, multiple teeth of the two-photon comb (Eq. (1) and Fig. 1**c** in the main text) can be used simultaneously to drive different hyperfine and fine-structure transitions in parallel at no cost in additional laser power (Fig. S1). In the limit that both the average and instantaneous excited state probabilities are small ($\Omega_N \ll \gamma < 2\pi f_{\text{r}}$) with unequal detunings from resonance for each transition being driven, coherences between multiple excited states can be neglected and each line will act essentially as an independent two-level system.

In Fig. S1, it is shown that that by choosing a comb tooth spacing of $f_{\text{r}} = 83.5$ MHz, all six of the allowed [6] hyperfine and fine structure transitions [7] on $1S{\rightarrow}3D$ can be driven simultaneously with a red detuning between $\gamma/3$ and $\gamma$. This illustrates the optical frequency comb's ability to act as its own hyperfine "repump," and allows this scheme to be applied robustly to magnetically trapped samples, where the presence of polarization imperfections or off-resonant excitation to undesired excited states can cause spin flips that must be repumped. Though not the focus of this work with two-photon transitions, we have verified experimentally that we can load and trap rubidium atoms in a one-photon optical frequency comb MOT that accomplishes its own hyperfine repumping with another tooth through judicious choice of the repetition rate.

Optical frequency combs at 205 nm with $\approx 100$ mW of time-averaged power and build-up cavity power enhancement factors of up to 10 have been demonstrated [8–11]. Focusing the intra-cavity 1 W beam to a spot size with diameter 60 $\mu$m to make a 1D optical molasses would produce a resonant excitation rate on $1S{\rightarrow}3D$ that is shown as a function of frequency in Fig. S1**a**. The photoionization rate at the peak scattering frequency would be $\gamma_{\text{ionization}} < 0.2\ \text{s}^{-1}$ under these circumstances, so each atom would be able to scatter thousands of photons before being ionized.

## DOPPLER LIMIT FOR TWO-PHOTON OPTICAL MOLASSES

To derive the Doppler cooling limit for (approximately equal frequency) two-photon transitions, we take an algebraic approach to derive one cooling and two heating mechanisms that will balance one another in equilibrium [12]. We

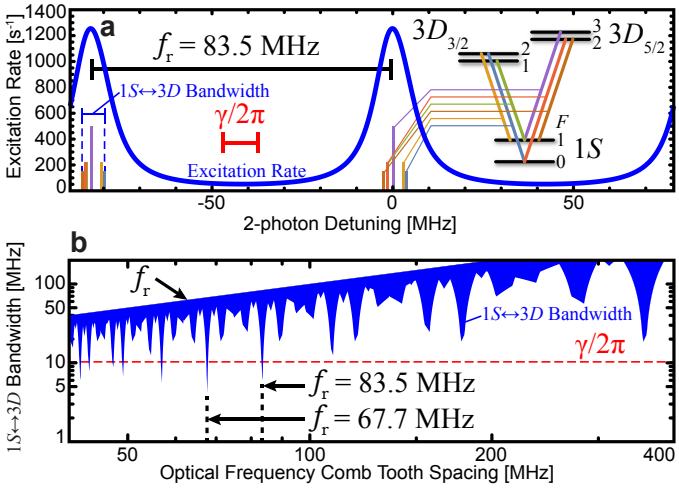


**Figure S1**. Calculated parameters for laser cooling atomic hydrogen on $1S \rightarrow 3D$. **a** Calculated excitation rate (blue) as a function of twice the optical frequency (the two-photon effective frequency at 102.5 nm) for a comb with repetition rate $f_r = 83.5$ MHz. The spectrum shown is the atomic spectrum modulo $f_r$, which is how the spectrum will appear when scanning a frequency comb. **b** The bandwidth spanned by the six allowed fine and hyperfine transition frequencies mod $f_r$ is less than the natural linewidth of $\gamma/2\pi = 10.3$ MHz for this repetition rate and a few others.

first derive the 1D Doppler cooling limit for two-photon laser cooling with a CW laser (or a comb with pulses colliding simultaneously on the atoms), then examine the situation for an optical frequency comb where there is some finite delay time that is longer than the pulse duration between forward and backward propagating pulses. We will assume that the two-photon transitions are driven well below saturation (resonant saturation parameter $s_N \ll 1$) and with a two-photon detuning of $\gamma/2$ to the red side of resonance. In the case of cooling with an optical frequency comb, we will assume that the single-tooth approximation discussed above is valid.

The average cooling force is given by the product of the momentum transfer per excitation and the excitation rate. In the limit where the Doppler shifts are small compared to the excited state linewidth, the cooling power is given by $\partial E/\partial t|_{\rm cool} = -s_N \hbar \omega_{\rm ge}^2 v^2/c^2$.

This cooling power is balanced by two sources of heating: heating due to randomly-distributed momentum kicks from absorption events and heating due to momentum kicks from spontaneous emission [12]. For the former, there are only contributions from the single-beam processes since two-beam absorption does not induce a momentum kick for counter-propagating beams, and the heating power from absorption is given by $\partial E/\partial t|_{\rm heat,abs.} = s_N \gamma \hbar^2 \omega_{\rm ge}^2/4mc^2$.

The second heating term is due to spontaneous emission and will depend upon the details of the decay channels available to the excited state. If the probability that an excited atom emits a photon with frequency $\omega_i$ at some point on its way to the ground state is $\mathcal{P}_i$, the heating from these decays can be modeled with a probability-weighted sum of the squares of the momentum kicks from these spontaneously-emitted photons, *viz.*

$$\left.\frac{\partial E}{\partial t}\right|_{\rm heat,spon.} = \frac{1}{2m}\gamma_{\rm tot}\sum_i \mathcal{P}_i \left(\hbar\frac{\omega_i}{c}\right)^2 \tag{S11}$$

where $\gamma_{\rm tot}$ is the total excitation rate (see *e.g.* Eq. (S10) for the case with a single beam from an optical frequency comb) and we are for the moment modeling the spontaneous emission as being confined to 1D, which gives a Doppler limit that agrees with the 3D calculation in the standard single-photon case.

Eq. (S11) shows the mechanism by which multi-photon cooling can give rise to a lower Doppler limit than single-photon cooling; by splitting the decay into smaller, uncorrelated momentum kicks, the mean square total momentum transfer (and therefore the heating) will on average be lower than for a single photon decay channel. Eq. (S11) also shows that there is an additional heating mechanism for the CW case since $\gamma_{\rm tot}$ will in this circumstance include two-beam excitations that are Doppler free for counter-propagating beams [4]. The excitation rate from the two-beam terms (which does not contribute to the cooling in 1D) is 4 times larger than each single-beam term, and the size of this effect for 1D two-photon laser cooling of atomic hydrogen on a quenched $1S \rightarrow 2S$ transition, for example, would lead to a comb-cooled Doppler temperature that is a factor of 2 lower than the predicted CW limit [4]. In order to make a quantitative estimate of the magnitude of these effects, we model the decay cascade as proceeding via a single

intermediate state halfway between $|\mathrm{g}\rangle$ and $|\mathrm{e}\rangle$ ($\mathcal{P}_i = 1$ and $\omega_i = \omega_{\mathrm{ge}}/2$ for $i = 1, 2$), which gives us

$$\left.\frac{\partial E}{\partial t}\right|_{\mathrm{heat,spon.}} = s_N \frac{3\gamma}{8} \frac{\hbar^2 \omega_{\mathrm{ge}}^2}{mc^2}. \tag{S12}$$

The equilibrium temperature at which the cooling and heating terms sum to zero for the CW case gives the Doppler limit for 2-photon 1D optical molasses with counter-propagating CW laser beams

$$T_{\mathrm{D,CW}} = \frac{5}{4} \frac{\gamma\hbar}{2k_{\mathrm{B}}}. \tag{S13}$$

This is 25% hotter than single-photon cooling on a transition with the same linewidth, despite the fact that it includes the reduction in heating from the cascade decay.

For the mode-locked case where pulses from the two directions do not collide on the atoms at the same time, the cooling power and heating power from absorption are both the same as the CW case in 1D. However, the heating power from spontaneous emission is reduced by a factor of 3 (compare Eq. (4) and Eq. (S12)) due to the absence of Doppler-free absorption, and the resulting Doppler cooling limit is given by Eq. (5), which is colder than both the CW and the single-photon cases.

We have extended this model to 3D and performed the detailed decay channel sum in Eq. (S11) for the rubidium transition used in this work and find that the calculated Doppler limit of $T_{\mathrm{D,comb}} = 12\ \mu$K agrees well with the prediction of Eq. (5).

## FINITE LASER TOOTH LINEWIDTH

By monitoring the 420 nm fluorescence from a hot vapor cell (Fig. 2a), a continuously-operating CW MOT (Fig. 2b), andthe pre-cooled (and then released) rubidium atoms as the ML laser frequency is swept (shown at the top of Fig. 3), we obtain a line shape that is more broad than the natural linewidth of $\gamma/2\pi = 667$ MHz [13]. For the latter, the Doppler broadening expected from motion would be 630 kHz if taken alone, and the magnetic field is zeroed to a level where magnetic broadening will not contribute to the spectral width. We find that, after taking into account the natural linewidth and the expected Doppler broadening, we have a residual FWHM of the two-photon spectrum of around 1.8 MHz, which we attribute to the laser. It is worth noting that using this width to infer an optical (that is, single-photon) comb tooth width or vice versa is highly dependent on the details of the broadening mechanism (see, *e.g.* [14]), and we therefore rely on the two-photon spectroscopy exclusively for determining our relevant effective two-photon spectral linewidth, which is model-independent. Combining this with the natural linewidth again via convolution gives us an effective two-photon spectral linewidth with a FWHM of $\gamma_{\mathrm{eff}}/2\pi = 2.2$ MHz.

To account for the effect of finite two-photon spectral linewidth on scattering rate, we approximate the line shape as Lorentzian to adopt the model of Haslwanter *et al.* [15], which in the low-intensity limit ($s_N \ll 1$) gives the scattering rate

$$\gamma_N = \frac{\Omega_N^2}{\gamma} \frac{\gamma/\gamma_{\mathrm{eff}}}{1 + \left(2\delta_N(\boldsymbol{v})/\gamma_{\mathrm{eff}}\right)^2}. \tag{S14}$$

We can recognize this as Eq. (3) with the replacement

$$\gamma \to \gamma_{\mathrm{eff}}, \tag{S15}$$

and conclude that a first approximation of the Doppler temperature limit can be made in the case of finite spectral linewidth by applying the replacement Eq. (S15) to expressions for the Doppler temperature (*e.g.* Eq. (5)). Using this approach for our experimental case where cooling is applied in 1D but spontaneous emission is approximated as being isotropic in 3D, we predict a Doppler limit of $T_{\mathrm{D,comb}} = 31\ \mu$K.

## FITTING ABSORPTION IMAGES FOR TEMPERATURE

The spatial width of an atomic cloud following Maxwell-Boltzmann statistics as a function of time, $t$, is

$$w(t) = \sqrt{w_0^2 + \frac{k_{\mathrm{B}}T}{m}t^2} \tag{S16}$$

where $w_0$ is the width at $t = 0$ when positions and velocities are uncorrelated. In Fig. 3 the temperature for data points labeled as "Free" are derived from fitting the free expansion to Eq. (S16) where $t = 0$ is defined as the end of CW laser cooling.

For the experiments shown in Fig. 3 in the main text, however, we illuminate the atoms with the ML laser at times $t > 0$ which introduces a damping force. The simple model of Eq. (S16) does not account for the extra dynamics resulting from optical forces. We therefore developed a simulation to model an expanding cloud of atoms (in three dimensions) that is subject to the optical forces of counterpropogating laser beams in one dimension. The data points marked "Constrained" in Fig. 3 in the main text are derived from analysis that relies on our simulation. For each temperature data point we input experiment parameters (detuning, initial sample temperature, initial sample width, ML cooling duration, etc.) along with the experimental measured widths of our atomic cloud during free expansion. We run the simulation multiple times as a function of scattering rate and select the simulation that minimizes $\chi^2$ between the experimentally measured widths and the simulation widths. From the best simulation we define a temperature using $T = \frac{m}{k_B}\sigma_v^2$ where $\sigma_v$ is the standard deviation of the simulation's velocity distribution. Despite the fact that the free expansion model does not include effects of the ML laser, the two methods give almost the same temperatures, which can be seen by comparing the blue and gray points in Fig. 3 in the main text and the black and red points in the inset of that figure. There seems to be a slightly higher inferred temperature when the monte carlo assisted analysis ("Constrained") is used in cases where the acceleration from the ML laser is large.


[1] S. Reinhardt, E. Peters, T. W. Hänsch, and Th. Udem, "Two-photon direct frequency comb spectroscopy with chirped pulses," Phys. Rev. A **81**, 033427 (2010).

[2] M. Haas, U. D. Jentschura, C. H. Keitel, N. Kolachevsky, M. Herrmann, P. Fendel, M. Fischer, Th. Udem, R. Holzwarth, T. W. Hänsch, M. O. Scully, and G. S. Agarwal, "Two-photon excitation dynamics in bound two-body coulomb systems including ac Stark shift and ionization," Phys. Rev. A **73**, 052501 (2006).

[3] Richard N. Zare, *Angular Momentum* (John Wiley and Sons, 1988).

[4] Véronique Zehnlé and Jean Claude Garreau, "Continuous-wave Doppler cooling of hydrogen atoms with two-photon transitions," Phys. Rev. A **63**, 021402(R) (2001).

[5] D. Kielpinski, "Laser cooling of atoms and molecules with ultrafast pulses," Phys. Rev. A **73**, 063407 (2006).

[6] Keith D. Bonin and Thomas J. McIlrath, "Two-photon electric-dipole selection rules," J. Opt. Soc. Am. B **1**, 52 (1984).

[7] A. E. Kramida, "A critical compilation of experimental data on spectral lines and energy levels of hydrogen, deuterium, and tritium," Atomic Data and Nuclear Data Tables **96**, 586 (2010).

[8] Kevin F. Wall, Joseph S. Smucz, Bhanana Pati, Yelena Isyanova, Peter F. Moulton, and Jeffrey G. Manni, "A quasi-continuous-wave deep ultraviolet laser source," IEEE Journal of Quantum Electronics **39**, 1160 (2003).

[9] Xin Zhang, Zhimin Wang, Guiling Wang, Yong Zhu, Zuyan Xu, and Chuangtian Chen, "Widely tunable and high-average-power fourth-harmonic generation of a Ti:sapphire laser with a $KBe_2BO_3F_2$ prism-coupled device," Optics Letters **34**, 1342 (2009).

[10] E. Peters, S. A. Diddams, P. Fendel, S. Reinhardt, T. W. Hänsch, and Th. Udem, "A deep-UV optical frequency comb at 205 nm," Optics Express **17**, 9183 (2009).

[11] Elisabeth Peters, Dylan C. Yost, Arthur Matveev, Theodor W. Hänsch, and Thomas Udem, "Frequency-comb spectroscopy of the hydrogen $1S$–$3S$ and $1S$–$3D$ transitions," Ann. Phys. (Berlin) **525**, L29 (2013).

[12] Christopher J. Foot, *Atomic Physics* (Oxford, 2005).

[13] D. Sheng, A. Pérez Galván, and L. A. Orozco, "Lifetime measurements of the $5d$ states of rubidium," Phys. Rev. A **78**, 062506 (2008).

[14] Robert E. Ryan, Lynn A. Westling, Reinhold Blümel, and Harold J. Metcalf, "Two-photon spectroscopy: A technique for characterizing diode-laser noise," Phys. Rev. A **52**, 3157 (1995).

[15] Th. Haslwanter, H. Ritsch, J. Cooper, and P. Zoller, "Laser-noise-induced population fluctuations in two- and three-level systems," Phys. Rev. A **38**, 5652 (1988).